

CrossMark  
click for updatesCite this: *RSC Adv.*, 2017, 7, 14186Received 18th January 2017  
Accepted 21st February 2017

DOI: 10.1039/c7ra00765e

rsc.li/rsc-advances

# La<sub>2</sub>Sn<sub>2</sub>O<sub>7</sub> enhanced photocatalytic CO<sub>2</sub> reduction with H<sub>2</sub>O by deposition of Au co-catalyst†

Shuang Chen, Bao Pan, Longquan Zeng, Shijian Luo, Xuxu Wang and Wenye Su\*

La<sub>2</sub>Sn<sub>2</sub>O<sub>7</sub> (LSO) micro/nanospheres, synthesized by a hydrothermal method, exhibited photocatalytic performance for CO<sub>2</sub> reduction. The evolution rate of the main reduction products (CH<sub>4</sub> and CO) was 0.20 and 0.10 μmol h<sup>-1</sup>, respectively. Loading of Au co-catalyst over La<sub>2</sub>Sn<sub>2</sub>O<sub>7</sub> efficiently enhanced the photocatalytic activity of CO<sub>2</sub> reduction. The highest photocatalytic efficiency was obtained over 1 wt% Au/La<sub>2</sub>Sn<sub>2</sub>O<sub>7</sub> with an apparent quantum yield (AQY) of 2.54%. Characterization techniques including SEM, TEM, XRD, XPS, DRS, PL, and electrochemical analysis were applied and the physicochemical properties of La<sub>2</sub>Sn<sub>2</sub>O<sub>7</sub> and Au/La<sub>2</sub>Sn<sub>2</sub>O<sub>7</sub> samples are discussed. A possible mechanism of photocatalytic CO<sub>2</sub> reduction over Au/La<sub>2</sub>Sn<sub>2</sub>O<sub>7</sub> is proposed.

## 1. Introduction

Because of the growing consumption of fossil fuels, atmospheric levels of carbon dioxide are greatly increasing thus causing tremendous concerns about ensuing effects on the global climate and future energy supplies. Research activities on the potential conversion of CO<sub>2</sub> are thus considerably stimulated.<sup>1,2</sup> Photocatalytic transformation of CO<sub>2</sub> is one of the most promising routes for the utilization of CO<sub>2</sub> because it can reduce CO<sub>2</sub> to hydrocarbon fuels, such as CH<sub>4</sub> and CH<sub>3</sub>OH, by solar energy in an environmentally friendly manner. Recently, various materials for photocatalytic CO<sub>2</sub>-reduction such as La<sub>2</sub>Ti<sub>2</sub>O<sub>7</sub>,<sup>3</sup> LaPO<sub>4</sub>,<sup>4–6</sup> TiO<sub>2</sub>,<sup>7–12</sup> C<sub>3</sub>N<sub>4</sub>,<sup>13–15</sup> ZnO,<sup>16</sup> Zn<sub>2</sub>GeO<sub>4</sub>,<sup>17</sup> TaON,<sup>18</sup> BaCeO<sub>3</sub>,<sup>19</sup> CdS<sup>20–23</sup> and metal complexes<sup>24</sup> have been reported, but with relatively low efficiencies. The synthesis of photocatalysts with high performance for CO<sub>2</sub> reduction has been a challenging – yet vital – research topic.

Semiconductors with a sufficiently more negative conduction band edge than the reduction potential of CO<sub>2</sub>, and with superior CO<sub>2</sub> adsorption capability, favour photocatalytic CO<sub>2</sub> reduction.<sup>4</sup> Lanthanum-based materials, due to a highly negative conduction band edge, may be suitable for efficient reduction of CO<sub>2</sub> with H<sub>2</sub>O<sup>25</sup> and alkaline lanthanum cations are considered to have efficient CO<sub>2</sub> adsorption sites.<sup>26</sup> Many lanthanum-based materials have been reported with photocatalytic performance for hydrogen production and

photocatalytic CO<sub>2</sub> reduction.<sup>5,7</sup> La<sub>2</sub>Sn<sub>2</sub>O<sub>7</sub>, as a key member of the lanthanum-based stannate family, possesses tailorable and tunable pyrochlore properties with high possibilities of leading to a wide variety of chemical and physical properties which could be applied as luminescent materials<sup>27</sup> and catalysts for different reactions.<sup>28,29</sup> Therefore, La<sub>2</sub>Sn<sub>2</sub>O<sub>7</sub> materials are expected to be promising candidates for CO<sub>2</sub>-reduction photocatalysts.

In the present study, a La<sub>2</sub>Sn<sub>2</sub>O<sub>7</sub> sample was prepared by a hydrothermal method and its photocatalytic performance for CO<sub>2</sub> reduction with H<sub>2</sub>O was investigated. Au nanoparticles were deposited on La<sub>2</sub>Sn<sub>2</sub>O<sub>7</sub> by a NaBH<sub>4</sub> reduction method in order to acquire higher photocatalytic CO<sub>2</sub> reduction efficiency. Synthesized La<sub>2</sub>Sn<sub>2</sub>O<sub>7</sub> and Au/La<sub>2</sub>Sn<sub>2</sub>O<sub>7</sub> samples were characterized by physical and chemical measurements and the effects of Au doping on photocatalytic performance are discussed. A possible reaction mechanism for photocatalysis on the prepared La<sub>2</sub>Sn<sub>2</sub>O<sub>7</sub> and Au/La<sub>2</sub>Sn<sub>2</sub>O<sub>7</sub> samples under UV light irradiation is also proposed.

## 2. Experimental

### 2.1. Catalyst preparation

La<sub>2</sub>Sn<sub>2</sub>O<sub>7</sub> was fabricated *via* a hydrothermal method. In a typical experiment, 2 mmol La(NO<sub>3</sub>)<sub>3</sub>·6H<sub>2</sub>O and 2 mmol Na<sub>2</sub>SnO<sub>3</sub> were dissolved in 40 mL DI water at room temperature with stirring to form a homogeneous solution. Then, Na<sub>2</sub>SnO<sub>3</sub> solution was added into the La(NO<sub>3</sub>)<sub>3</sub> solution drop by drop with vigorous stirring. The resulting suspension was transferred into a 100 mL Teflon-lined stainless steel autoclave and hydrothermally treated at 200 °C for 12 h, and then cooled naturally. The precipitate was collected by centrifugation and washed several times with distilled water before drying at 60 °C to obtain the final product. Au nanoparticles were

State Key Laboratory of Photocatalysis on Energy and Environment, Fuzhou University, Fuzhou 350002, P. R. China. E-mail: suweny@fzu.edu.cn; Fax: +86-591-83779105; Tel: +86-591-83779105

† Electronic supplementary information (ESI) available: XPS survey spectrum of the 1 wt% Au/La<sub>2</sub>Sn<sub>2</sub>O<sub>7</sub> sample; N<sub>2</sub> adsorption/desorption isotherms (77 K) of La<sub>2</sub>Sn<sub>2</sub>O<sub>7</sub> and 1 wt% Au/La<sub>2</sub>Sn<sub>2</sub>O<sub>7</sub> samples; the stability test of 1 wt% Au/La<sub>2</sub>Sn<sub>2</sub>O<sub>7</sub> photocatalyst for CH<sub>4</sub>, CO, H<sub>2</sub> evolution rate in four repeats of reaction. See DOI: 10.1039/c7ra00765e



deposited on the surface of  $\text{La}_2\text{Sn}_2\text{O}_7$  ( $\text{Au}/\text{La}_2\text{Sn}_2\text{O}_7$ ) by a  $\text{NaBH}_4$  reduction method. The  $\text{La}_2\text{Sn}_2\text{O}_7$  powders were dissolved in 100 mL  $\text{H}_2\text{O}$  by ultrasonic dispersion and an appropriate volume of  $\text{HAuCl}_4$  solution ( $5 \text{ mg Au mL}^{-1}$ ) was added. After vigorous stirring for 12 hours, the resulting mixture was reduced with  $\text{NaBH}_4$  solution ( $0.1 \text{ M}$ ), then centrifuged and washed thoroughly with distilled water, and dried at  $60^\circ\text{C}$  for 12 h. The gold contents of the samples were estimated by precursor feeding. The values for the actual Au loading of the synthesized catalysts were obtained by using an inductively coupled plasma mass spectrometer (ICP-MS, OPTIMA 8000), and summarized in Table S1.<sup>†</sup>

## 2.2. Characterization

Powder X-ray diffraction (XRD) data was collected using a Bruker D8 Advance instrument ( $\text{Cu K}\alpha 1$  irradiation,  $\lambda = 1.5406 \text{ \AA}$ ). Morphological images of the surfaces and transmission electron micrographs were obtained using a Nova NanoSEM 230 microscope (FEI Corp) and a JEOL JEM 2010F microscope. UV-vis

irradiation quartz reaction cell inside of it. 50 mg photocatalyst was added into the quartz reactor and dispersed in 140 mL  $\text{H}_2\text{O}$ . A 125 W high-pressure mercury lamp (GGZ125, Shanghai Yaming Lighting Co, Ltd with a maximum emission at about 365 nm) was used as the light source and the reactor was kept invariably at  $20^\circ\text{C}$  by flowing cooling water during the reaction process. The whole reaction system was first evacuated by a mechanical pump to remove air before irradiation, then  $\text{CO}_2$  (99.999% purity) was introduced into the reactor for 40 minutes to establish an adsorption-desorption balance and provide the necessary reaction gas. Gas products were detected by GC (Agilent 6890N) and the apparent quantum yield (AQY) was also measured under the same photocatalytic reaction conditions. The incident light intensity of a high pressure mercury lamp was measured by Spectri Light ILT950. The total number of incident photons was collected by a calibrated silicon photodiode.

The apparent quantum yield (AQY) was calculated from the following equations:

$$\text{AQY}(\%) = \frac{\text{number of reacted electrons}}{\text{number of incident photons}} \times 100\%$$

$$= \frac{\text{number of CH}_4 \text{ molecules} \times 8 + \text{number of H}_2 \text{ molecules} \times 2 + \text{number of CO molecules} \times 2}{\text{number of incident photons}} \times 100\%$$

diffuse reflectance spectra (DRS) were measured using a Varian Cary 500 Scan, with  $\text{BaSO}_4$  as a reference. X-ray photoelectron spectroscopy (XPS) measurements were performed on an ESCALAB 250 photoelectron spectroscope system. Brunauer-Emmett-Teller (BET) specific surface area and  $\text{CO}_2$  adsorption were recorded using an ASAP2020M apparatus. Electrochemical experiments were performed in a three-electrode cell made of quartz. A Pt plate and  $\text{Ag}/\text{AgCl}$  electrode served as the counter electrode and reference electrode, respectively. The working electrode was made by dip-coating a catalyst slurry ( $10 \text{ mg mL}^{-1}$  in  $\text{EtOH}$ ) on fluorine-doped tin oxide (FTO) glasses, whose area was set as *ca.*  $0.5 \text{ cm} \times 0.5 \text{ cm}$ , and then was air-dried naturally. Electrochemical experiments were determined by a Zennium electrochemical workstation (Zahner Elektrik, Germany). The Mott-Schottky experiments and photocurrent response behaviors were conducted on a Precision PARC workstation. A  $0.2 \text{ M Na}_2\text{SO}_4$  aqueous solution was used as the electrolyte for the two experiments. A 300 W Xe lamp (CEL-S500/350) was utilized as the light source for the photocurrent response behavior test. Electrochemical impedance spectroscopy (EIS) experiments were conducted on a CHI660D workstation (CH instrument) in an electrolyte of  $0.5 \text{ M KCl}$  aqueous solution containing  $0.01 \text{ M K}_3[\text{Fe}(\text{CN})_6]/\text{K}_4[\text{Fe}(\text{CN})_6]$  ( $1:1$ ). Photoluminescence (PL) spectra were carried out on an Edinburgh instrument FLS980 spectrophotometer at ambient conditions.

## 2.3. Photocatalytic reactions

Photocatalytic reactions for  $\text{CO}_2$  reduction were carried out at 1 atm  $\text{CO}_2$  partial pressure in a 200 mL reactor, with an

## 3. Results and discussion

### 3.1. Characterization of $\text{La}_2\text{Sn}_2\text{O}_7$ and $\text{Au}/\text{La}_2\text{Sn}_2\text{O}_7$

XRD patterns of the  $\text{La}_2\text{Sn}_2\text{O}_7$  and  $\text{Au}/\text{La}_2\text{Sn}_2\text{O}_7$  samples are shown in Fig. 1. The four characteristic peaks located at  $28.8^\circ$ ,  $33.4^\circ$ ,  $48.0^\circ$ , and  $57.0^\circ$  are indexed to the (222), (400), (440), and (622) diffraction planes of cubic crystalline  $\text{La}_2\text{Sn}_2\text{O}_7$  (JCPDS: 73-1686), respectively. The average crystal size of the  $\text{La}_2\text{Sn}_2\text{O}_7$  sample is estimated to be about 14.5 nm from the (222) peak at around  $28.8^\circ$  by using the Scherrer equation. Diffraction peaks of the  $\text{Au}/\text{La}_2\text{Sn}_2\text{O}_7$  sample ascribe only to the cubic phase of  $\text{La}_2\text{Sn}_2\text{O}_7$ , and no diffraction peaks for Au were observed. This is due to a lower amount

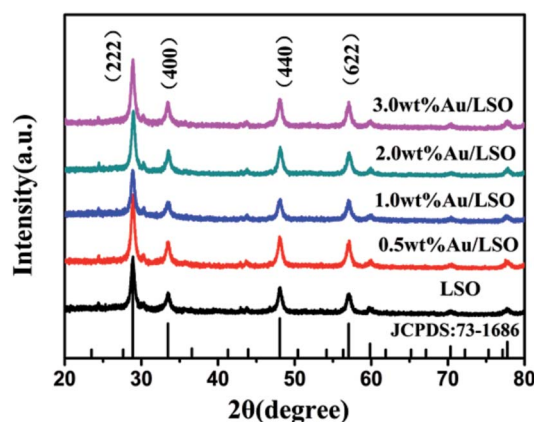


Fig. 1 XRD patterns of the  $\text{La}_2\text{Sn}_2\text{O}_7$  and  $\text{Au}/\text{La}_2\text{Sn}_2\text{O}_7$  samples.



of metal loading and homogenous dispersion of Au on the  $\text{La}_2\text{Sn}_2\text{O}_7$ .

Morphology and sizes of the samples were characterized by SEM and TEM. The  $\text{La}_2\text{Sn}_2\text{O}_7$  sample shows micro/nanospheres with diameters that varied from 300 to 500 nm, assembled by densely arranged nanoparticles (Fig. 2a). The TEM of the 1 wt% Au/ $\text{La}_2\text{Sn}_2\text{O}_7$  sample indicates few Au NPs dispersed on the  $\text{La}_2\text{Sn}_2\text{O}_7$  surface (Fig. 2b). The HRTEM image of the 1 wt% Au/ $\text{La}_2\text{Sn}_2\text{O}_7$  sample (Fig. 2c) shows a lattice spacing of *ca.* 0.234 nm, corresponding to the (111) planes of Au NPs,<sup>30,31</sup> and the size of the Au particle is about 5–7 nm. Meanwhile, the lattice spacing of the  $\text{La}_2\text{Sn}_2\text{O}_7$  structure is *ca.* 0.309 nm, corresponding to the (222) plane of cubic  $\text{La}_2\text{Sn}_2\text{O}_7$ . Furthermore, the obtained EDX pattern corresponding to Fig. 2d shows the presence of La, Sn, O, Au, and Cu elements (Cu peaks arise from TEM grid), and the obtained EDX-mapping (Fig. S1†) shows uniform distribution of the elements.

An X-ray photoelectron spectroscopy (XPS) survey spectrum of the prepared 1 wt% Au/ $\text{La}_2\text{Sn}_2\text{O}_7$  sample (Fig. S2†) indicates the presence of La, Sn, O, and Au. No other element signal is found except for a C signal (attributed to adventitious carbon), in accord with the results of EDX (Fig. 2d). In the high resolution XPS spectrum of Au 4f (Fig. 3a), two main peaks located at 82.7 and 86.4 eV correspond to  $\text{Au}^0$  4f<sub>7/2</sub> and  $\text{Au}^0$  4f<sub>5/2</sub>.<sup>32</sup> And the  $\text{Au}^0$  4f<sub>7/2</sub> negative binding energy shift of 1.4 eV, compared with that of bulk metallic  $\text{Au}^0$  (84.1 eV), indicates strong interactions between Au and  $\text{La}_2\text{Sn}_2\text{O}_7$ .<sup>33</sup> With regard to La 3d (Fig. 3b), the binding energies of La 3d<sub>5/2</sub> and La 3d<sub>3/2</sub> peaks are present at 836.1 and 853.2 eV with the shake-up peaks located at 840.2 and 857.3 eV, respectively, consistent with the reported results of  $\text{La}^{3+}$  in a  $\text{La(III)}$  oxidation state.<sup>34</sup> The Sn 3d XPS spectra (Fig. 3c) show two main peaks at 486.2 eV (Sn 3d<sub>5/2</sub>) and 494.7 eV (Sn 3d<sub>3/2</sub>) with the shake-up peaks located at 488.3 and 496.7 eV,<sup>35</sup> which may be assigned to the characteristic of  $\text{Sn}^{4+}$ . As for O 1s XPS spectra (Fig. 3d), the O 1s signal could be fit into two peaks, and the peaks located at 528.7 and 531.2 eV are ascribed to the crystal lattice oxygen and surface hydroxyl, respectively.<sup>36</sup>

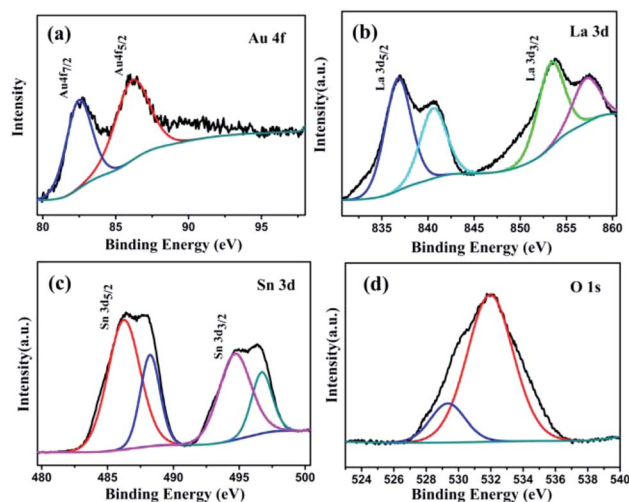


Fig. 3 XPS spectra of the 1 wt% Au/ $\text{La}_2\text{Sn}_2\text{O}_7$  sample: (a) Au element; (b) La element; (c) Sn element; and (d) O element.

The UV-vis diffused reflection spectra of the samples are shown in Fig. 4. Onset of the absorption edge for the  $\text{La}_2\text{Sn}_2\text{O}_7$  is at about 315 nm. The corresponding bandgap energy ( $E_g$ ) is estimated to be 3.93 eV, as determined by equation  $E = 1240/\lambda$ . Compared to bare  $\text{La}_2\text{Sn}_2\text{O}_7$  materials, the absorption edge of Au/ $\text{La}_2\text{Sn}_2\text{O}_7$  samples does not change, suggesting that Au is only loaded on the surface of  $\text{La}_2\text{Sn}_2\text{O}_7$  rather than being incorporated into the lattice of  $\text{La}_2\text{Sn}_2\text{O}_7$ .<sup>37</sup> Meanwhile, an intense absorption band is centered at 531 nm, which could be assigned to the SPR of the Au NPs.<sup>38</sup> It can be seen that Au loading enhances the light absorption of  $\text{La}_2\text{Sn}_2\text{O}_7$  samples, and the absorption intensity heightens along with increased Au doping amounts.

The BET surface area ( $S_{\text{BET}}$ ) of the prepared samples was investigated by  $\text{N}_2$  adsorption-desorption measurements. The  $S_{\text{BET}}$  of the as-prepared  $\text{La}_2\text{Sn}_2\text{O}_7$  and 1 wt% Au/ $\text{La}_2\text{Sn}_2\text{O}_7$  were measured to be 75.6 and 70.6  $\text{m}^2 \text{g}^{-1}$  (Fig. S3†), respectively. The wide pore size distribution curves (Fig. S4†) indicate stacking among the small  $\text{La}_2\text{Sn}_2\text{O}_7$  nanoparticles. Meanwhile,  $\text{CO}_2$  adsorption over the samples was also measured and results are

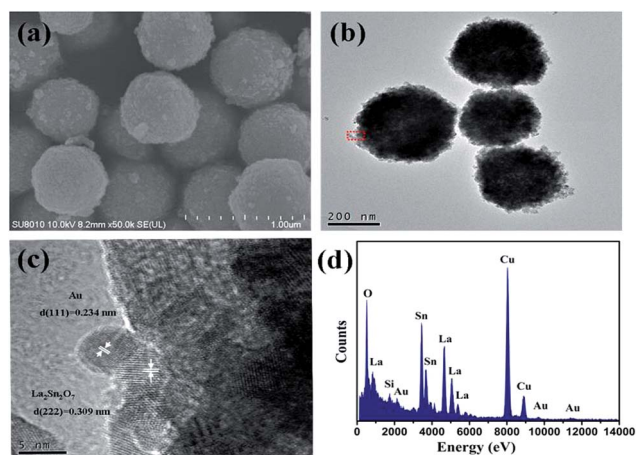


Fig. 2 (a) SEM image of the  $\text{La}_2\text{Sn}_2\text{O}_7$  sample; (b) TEM image; (c) HRTEM image; (d) EDX pattern of the 1 wt% Au/ $\text{La}_2\text{Sn}_2\text{O}_7$  sample.

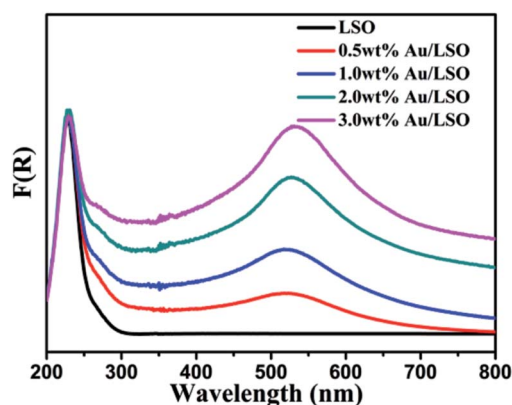


Fig. 4 The UV-vis diffused reflection spectra of  $\text{La}_2\text{Sn}_2\text{O}_7$  and Au/ $\text{La}_2\text{Sn}_2\text{O}_7$  samples.



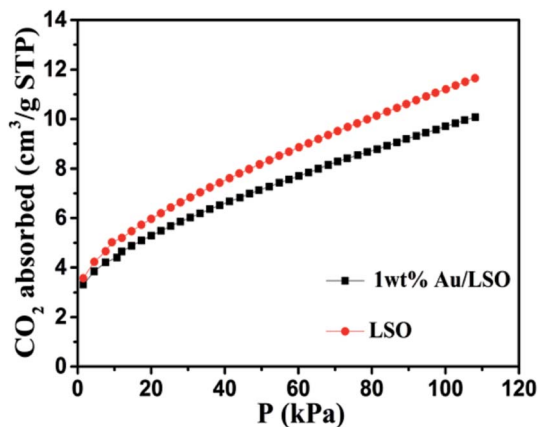


Fig. 5  $\text{CO}_2$  adsorption isotherms of  $\text{La}_2\text{Sn}_2\text{O}_7$  and 1 wt%  $\text{Au}/\text{La}_2\text{Sn}_2\text{O}_7$  samples.

shown in Fig. 5. The  $\text{CO}_2$  adsorption amounts of the  $\text{La}_2\text{Sn}_2\text{O}_7$  and 1 wt%  $\text{Au}/\text{La}_2\text{Sn}_2\text{O}_7$  samples are 11.65 and  $10.07 \text{ cm}^3 \text{ g}^{-1}$  (Fig. 5), respectively. 1 wt%  $\text{Au}/\text{La}_2\text{Sn}_2\text{O}_7$  shows a lower  $\text{CO}_2$  adsorption capability compared to  $\text{La}_2\text{Sn}_2\text{O}_7$ , which may be due to some surface  $\text{CO}_2$  adsorption sites, such as La species over  $\text{La}_2\text{Sn}_2\text{O}_7$ , that are covered with deposited Au nanoparticles.<sup>39</sup>

As shown in Fig. 6, the flat-band potential of  $\text{La}_2\text{Sn}_2\text{O}_7$  determined from Mott–Schottky plots is *ca.*  $-0.89 \text{ V vs. Ag/AgCl}$  at pH 7 (equivalent to  $-0.69 \text{ V vs. NHE}$  at pH 7). The positive slopes of these plots suggest that  $\text{La}_2\text{Sn}_2\text{O}_7$  is an n-type semiconductor.<sup>40</sup> With regard to the n-type semiconductor, the conduction band lies very close to the flat-band potentials.<sup>41</sup> Therefore, the conduction band ( $E_{\text{CB}}$ ) of  $\text{La}_2\text{Sn}_2\text{O}_7$  is  $-0.79 \text{ V vs. NHE}$  at pH 7, which is more negative than the redox potential of  $\text{CO}_2/\text{CO}$  ( $-0.53 \text{ V vs. NHE}$ ),  $\text{CO}_2/\text{CH}_4$  ( $-0.24 \text{ V vs. NHE}$ ), and  $\text{H}_2\text{O}/\text{H}_2$  ( $-0.41 \text{ V vs. NHE}$ ). So, it is thermodynamically possible that the photogenerated electrons in the prepared  $\text{La}_2\text{Sn}_2\text{O}_7$  reduce  $\text{CO}_2$  with  $\text{H}_2\text{O}$  to  $\text{CO}$ ,  $\text{CH}_4$ , and  $\text{H}_2$ .

### 3.2. Photocatalytic activity and stability

Photocatalytic  $\text{CO}_2$  reduction activities of the samples were investigated under mild conditions without any sacrificial

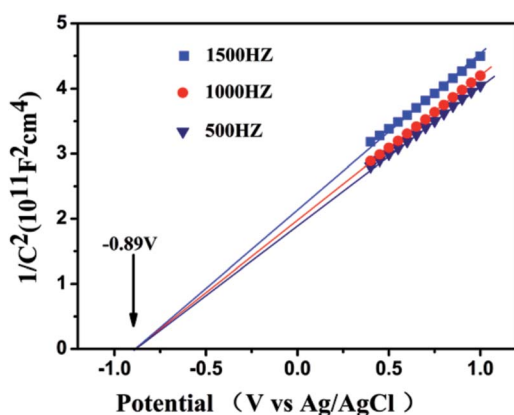


Fig. 6 Mott–Schottky plots of  $\text{La}_2\text{Sn}_2\text{O}_7$ .

reagents. As shown in Fig. 7a, the samples exhibited photocatalytic performance for  $\text{CO}_2$  reduction with  $\text{H}_2\text{O}$ , and  $\text{CH}_4$ ,  $\text{CO}$ , and  $\text{H}_2$  are the main reduction products; other products such as  $\text{CH}_3\text{OH}$ ,  $\text{HCHO}$ , and  $\text{HCOOH}$  were not detected during the reaction. The output products of  $\text{CH}_4$ ,  $\text{CO}$ , and  $\text{H}_2$ , over bare  $\text{La}_2\text{Sn}_2\text{O}_7$  were 0.60, 0.31, and  $6.90 \mu\text{mol}$  after 3 h irradiation, corresponding to the evolution rates of 0.20, 0.10, and  $2.30 \mu\text{mol h}^{-1}$ , respectively, with an apparent quantum yield (AQY) of 0.89%, which is superior to the P25 sample with a AQY of 0.68% (Table S2†). After loading Au, the samples exhibited better photocatalytic  $\text{CO}_2$  reduction activities. The evolution rate of the main products increased with addition of Au. When the loading amount of Au reached 1.0 wt%, the evolution rate of  $\text{CH}_4$ ,  $\text{CO}$ , and  $\text{H}_2$  increased to the max of 0.43, 0.37, and  $6.98 \mu\text{mol h}^{-1}$ , respectively (Fig. 7b), which was 2.2, 3.7, and 3.0 times as high as that of bare  $\text{La}_2\text{Sn}_2\text{O}_7$ . The generation of  $\text{H}_2$ ,  $\text{CH}_4$ , and  $\text{CO}$  over 1.0 wt%  $\text{Au}/\text{La}_2\text{Sn}_2\text{O}_7$  increased almost linearly with irradiation time (Fig. 7b), and their outputs are 2.05, 1.74, and  $33.08 \mu\text{mol}$  after 5 h irradiation, respectively, with an apparent quantum yield (AQY) (2.54%) enhanced by 3 times more than the  $\text{La}_2\text{Sn}_2\text{O}_7$  sample.

The amount of  $\text{O}_2$  formed was also measured to determine charge balance during the photocatalytic reaction. After a 5 h photocatalytic reaction over the 1.0 wt%  $\text{Au}/\text{La}_2\text{Sn}_2\text{O}_7$  sample, the amount of  $\text{O}_2$  was  $21.08 \mu\text{mol}$ . Supposing that the oxidation of  $\text{H}_2\text{O}$  to  $\text{O}_2$  is the only reaction to expend the photogenerated holes, and the photogenerated electrons are used to form  $\text{CH}_4$ ,  $\text{CO}$ , and  $\text{H}_2$ , then the stoichiometric molar ratio of  $\text{O}_2/(4\text{CH}_4 + \text{H}_2 + \text{CO})$  should be 0.5. The molar ratio of  $\text{O}_2/(4\text{CH}_4 + \text{H}_2 + \text{CO})$  calculated from our results is 0.49, which is reasonably close to the stoichiometric ratio.

Stability is very important for practical photocatalytic systems; thus cyclic testing of the photocatalytic  $\text{CO}_2$  reduction activities was performed to investigate stability. During the 4 times repeated reaction cycles of a 1 wt%  $\text{Au}/\text{La}_2\text{Sn}_2\text{O}_7$  sample (Fig. S5†), there was no distinct decrease in  $\text{H}_2$ ,  $\text{CH}_4$ , and  $\text{CO}$  evolution rates, thus demonstrating that the 1 wt%  $\text{Au}/\text{La}_2\text{Sn}_2\text{O}_7$  sample shows considerable photostability.

Control experiments were also carried out. No product was detected in the reaction system in the dark or without catalyst, indicating that the  $\text{CO}_2$  reduction requires presence of a photocatalyst. Only  $\text{H}_2$  was detected when  $\text{CO}_2$  was replaced by high purity  $\text{N}_2$  in the reaction system. This result suggests that the

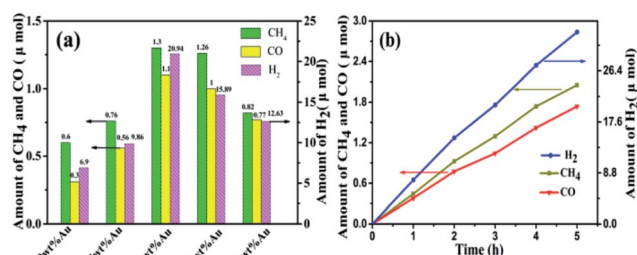


Fig. 7 (a) The output of  $\text{CH}_4$ ,  $\text{CO}$ , and  $\text{H}_2$  over  $\text{La}_2\text{Sn}_2\text{O}_7$  and  $\text{Au}/\text{La}_2\text{Sn}_2\text{O}_7$  samples under irradiation for 3 h; (b)  $\text{CH}_4$ ,  $\text{CO}$ , and  $\text{H}_2$  formed as a function of irradiation time over 1 wt%  $\text{Au}/\text{La}_2\text{Sn}_2\text{O}_7$  samples.

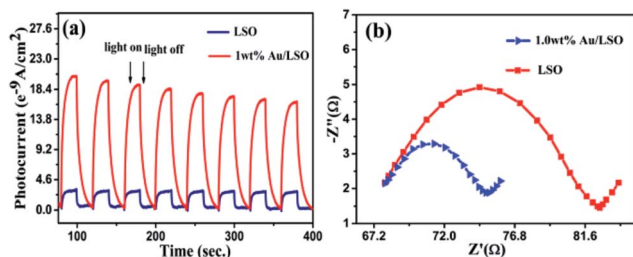


Fig. 8 (a) Transient photocurrent response; (b) Nyquist plots of  $\text{La}_2\text{Sn}_2\text{O}_7$  and 1 wt% Au/ $\text{La}_2\text{Sn}_2\text{O}_7$  samples.

formed reduced products originated from  $\text{CO}_2$  and not from other sources of contamination.

### 3.3. Photocatalytic mechanism

Transient photocurrent responses of the  $\text{La}_2\text{Sn}_2\text{O}_7$  and 1 wt% Au/ $\text{La}_2\text{Sn}_2\text{O}_7$  samples were measured under intermittent UV-vis illumination. As shown in Fig. 8a, the transient photocurrent of a 1 wt% Au/ $\text{La}_2\text{Sn}_2\text{O}_7$  sample was much higher than that of the bare  $\text{La}_2\text{Sn}_2\text{O}_7$ , indicating a more efficient separation and longer lifetime of photogenerated charge carriers with the loading of Au.<sup>42</sup> It has been proven that a smaller arc radius in a Nyquist plot implies a more effective charge separation of electron-hole pairs and a faster interfacial charge transfer.<sup>43,44</sup> The impedance arc of 1 wt% Au/ $\text{La}_2\text{Sn}_2\text{O}_7$  is much smaller than that of  $\text{La}_2\text{Sn}_2\text{O}_7$  (Fig. 8b), corresponding to its higher speed of charge separation of electron-hole pairs and interfacial charge transfer, which agrees well with their photocatalytic performances as discussed above. Meanwhile, photoluminescence spectra of the  $\text{La}_2\text{Sn}_2\text{O}_7$  and 1 wt% Au/ $\text{La}_2\text{Sn}_2\text{O}_7$  samples with an excitation wavelength of 310 nm are shown in Fig. 9. A strong PL emission spectrum centered around 410 nm is observed over the  $\text{La}_2\text{Sn}_2\text{O}_7$ , which comes from a trap-state emission, originating from the anion ( $\text{O}^{2-}$ ) or cation ( $\text{La}^{3+}$  and  $\text{Sn}^{4+}$ ) vacancy defects, and other crystallographic defects.<sup>45</sup> After loading Au on  $\text{La}_2\text{Sn}_2\text{O}_7$ , the emission intensity remarkably decreases, indicating enhancement of the separation and transfer of photo-generated electrons and holes. This result also is in accordance with the photocurrent performance. All the observations above highlight the function of the Au co-catalyst for enhancing charge transfer, leading to a higher photocatalytic efficiency.

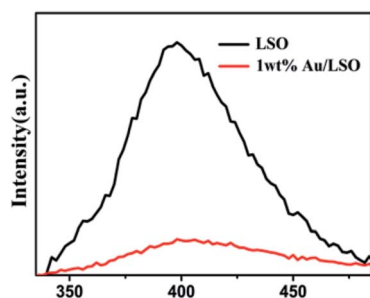


Fig. 9 Photoluminescence (PL) spectra of  $\text{La}_2\text{Sn}_2\text{O}_7$  and 1 wt% Au/ $\text{La}_2\text{Sn}_2\text{O}_7$  samples collected at the excitation wavelength of 310 nm.

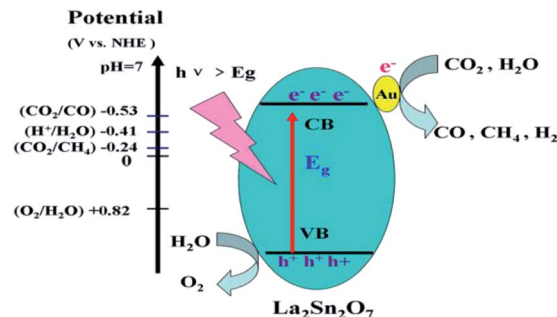


Fig. 10 Proposed mechanism of photocatalytic  $\text{CO}_2$  reduction over  $\text{La}_2\text{Sn}_2\text{O}_7$  with Au co-catalyst.

The mechanism for  $\text{CO}_2$  reduction with  $\text{H}_2\text{O}$  over Au/ $\text{La}_2\text{Sn}_2\text{O}_7$  is proposed as shown in Fig. 10. When light with photon energy higher or equal to the band gap of  $\text{La}_2\text{Sn}_2\text{O}_7$  is incident on the sample, then electrons and holes are generated in the CB and VB, respectively. Photogenerated electrons on the CB are transferred to the absorbed  $\text{CO}_2$  and  $\text{H}^+$  to produce  $\text{CH}_4$ ,  $\text{CO}$  or  $\text{H}_2$  on the surface of  $\text{La}_2\text{Sn}_2\text{O}_7$ . Simultaneously, holes on the VB edge of  $\text{La}_2\text{Sn}_2\text{O}_7$  are positive enough to oxidize water to form  $\text{O}_2$ . The deposited Au acts as a co-catalyst which facilitates transfer of photoexcited electrons and prevents the recombination of photoexcited electrons and holes.

## 4. Conclusion

$\text{La}_2\text{Sn}_2\text{O}_7$  micro/nanospheres were successfully synthesized by a facile hydrothermal method and Au nanoparticles were deposited on  $\text{La}_2\text{Sn}_2\text{O}_7$  via  $\text{H}_2\text{AuCl}_6$  impregnation followed by  $\text{NaBH}_4$  reduction. The prepared  $\text{La}_2\text{Sn}_2\text{O}_7$  sample showed photocatalytic  $\text{CO}_2$  reduction activities and  $\text{CH}_4$ ,  $\text{CO}$ , and  $\text{H}_2$  were the main reduction products. Deposition of an Au co-catalyst significantly improved photocatalytic performance. The highest evolution rates of  $\text{CH}_4$ ,  $\text{CO}$ , and  $\text{H}_2$  were observed over 1.0 wt% Au/ $\text{La}_2\text{Sn}_2\text{O}_7$  samples with 0.43, 0.37, and 6.98  $\mu\text{mol h}^{-1}$ , respectively. The apparent quantum yield (AQY) was 2.54%, which was enhanced by 3 times in contrast to bare  $\text{La}_2\text{Sn}_2\text{O}_7$ . An Au co-catalyst plays an excellent role as an electron transfer mediator. Our results indicate promising application of the  $\text{La}_2\text{Sn}_2\text{O}_7$  photocatalyst for  $\text{CO}_2$  reduction. Moreover, Au nanoparticles could be superior candidates for a co-catalyst to enhance  $\text{CO}_2$  reduction activities.

## Acknowledgements

This work was financially supported by the NSFC (Grants No. U1305242, 21373050), the National Key Basic Research Program of China (973 Program: 2013CB632405, 2014CB239303, 2014CB260410, 2014BAC13B03).

## Notes and references

- 1 L. Yuan and Y. J. Xu, *Appl. Surf. Sci.*, 2015, **342**, 154–167.



- 2 E. V. Kondratenko, G. Mul, J. Baltrusaitis, G. O. Larrazabal and J. Perez-Ramirez, *Energy Environ. Sci.*, 2013, **6**, 3112–3135.
- 3 Z. Wang, K. Teramura, S. Hosokawa and T. Tanaka, *Appl. Catal., B*, 2015, **163**, 241–247.
- 4 B. Pan, S. J. Luo, W. Y. Su and X. X. Wang, *Appl. Catal., B*, 2015, **168**, 458–464.
- 5 B. Pan, Y. G. Zhou, W. Y. Su and X. X. Wang, *Nano Res.*, 2017, **10**, 534–545.
- 6 B. Pan, Y. G. Zhou, W. Y. Su and X. X. Wang, *RSC Adv.*, 2016, **6**, 34744–34747.
- 7 C. Xu, X. P. He, C. Wang, X. Chen, R. S. Yuan and W. X. Dai, *RSC Adv.*, 2016, **6**, 84068–84073.
- 8 A. Sarkar, E. Gracia-Espino, T. Wagberg, A. Shchukarev, M. Mohl, A. R. Rautio, O. Pitkanen, T. Sharifi, K. Kordas and J. P. Mikkola, *Nano Res.*, 2016, **9**, 1956–1968.
- 9 M. Wang, Q. T. Han, Y. Zhou, P. Li, W. G. Tu, L. Q. Tang and Z. G. Zou, *RSC Adv.*, 2016, **6**, 81510–81516.
- 10 M. S. Akple, J. X. Low, S. W. Liu, B. Cheng, J. G. Yu and W. K. Ho, *J. CO<sub>2</sub> Util.*, 2016, **16**, 442–449.
- 11 M. Tahir, B. Tahir and N. A. S. Amin, *Appl. Surf. Sci.*, 2015, **356**, 1289–1299.
- 12 O. Ola and M. M. Maroto-Valer, *J. Photochem. Photobiol., C*, 2015, **24**, 16–42.
- 13 J. N. Qin, S. B. Wang, H. Ren, Y. D. Hou and X. C. Wang, *Appl. Catal., B*, 2015, **179**, 1–8.
- 14 W. J. Ong, L. K. Putri, L. L. Tan, S. P. Chai and S. T. Yong, *Appl. Catal., B*, 2016, **180**, 530–543.
- 15 W. L. Yu, D. F. Xu and T. Y. Peng, *J. Mater. Chem. A*, 2015, **3**, 19936–19947.
- 16 T. Wang, L. Shi, J. Tang, V. Malgras, S. Asahinja, G. G. Liu, H. B. Zhang, X. G. Meng, K. Chang, J. P. He, O. Terasaki, Y. Yamauchi and J. H. Ye, *Nanoscale*, 2016, **8**, 6712–6720.
- 17 Q. Liu, Y. Zhou, Z. P. Tian, X. Y. Chen, J. Gao and Z. G. Zou, *J. Mater. Chem.*, 2012, **22**, 2033–2038.
- 18 Q. T. Han, Y. Zhou, L. Q. Tang, P. Li, W. G. Tu, L. Li, H. J. Lia and Z. G. Zou, *RSC Adv.*, 2016, **6**, 90792–90796.
- 19 J. Wang, C. X. Huang, X. L. Chen, H. T. Zhang, Z. S. Li and Z. G. Zou, *Appl. Surf. Sci.*, 2015, **358**, 463–467.
- 20 S. B. Wang and X. C. Wang, *Appl. Catal., B*, 2015, **162**, 494–500.
- 21 J. G. Yu, J. Jin, B. Cheng and M. Jaroniec, *J. Mater. Chem. A*, 2014, **2**, 3407–3416.
- 22 J. Jin, J. G. Yu, D. P. Guo, C. Cui and W. K. Ho, *Small*, 2015, **11**, 5262–5271.
- 23 S. Ijaz, M. F. Ehsan, M. N. Ashiq, N. Karamat and T. He, *Appl. Surf. Sci.*, 2016, **390**, 550–559.
- 24 Y. Yamazaki, H. Takeda and O. Ishitani, *J. Photochem. Photobiol., C*, 2015, **25**, 106–137.
- 25 Y. Xu and M. A. A. Schoonen, *Am. Mineral.*, 2000, **85**, 543–556.
- 26 S. P. Wang, S. L. Yan, X. B. Ma and J. L. Gong, *Energy Environ. Sci.*, 2011, **4**, 3805–3819.
- 27 J. Yang, Y. Su, H. Li, X. Liu and Z. Chen, *J. Alloys Compd.*, 2011, **509**, 8008–8012.
- 28 S. Park, *Solid State Ionics*, 2004, **175**, 625–629.
- 29 J. Zeng, H. Wang, Y. C. Zhang, M. K. Zhu and H. Yan, *J. Phys. Chem. C*, 2007, **111**, 11879–11887.
- 30 Z. Y. Zhang, Z. Wang, S. W. Cao and C. Xue, *J. Phys. Chem. C*, 2013, **117**, 25939–25947.
- 31 B. J. Borah, S. J. Borah, K. Saikia and D. K. Dutta, *Catal. Sci. Technol.*, 2014, **4**, 4001–4009.
- 32 W. B. Hou, W. H. Hung, P. Pavaskar, A. Goepfert, M. Aykol and S. B. Cronin, *ACS Catal.*, 2011, **1**, 929–936.
- 33 F. L. Wang, Y. J. Jiang, D. J. Lawes, G. E. Ball, C. F. Zhou, Z. W. Liu and R. Amal, *ACS Catal.*, 2015, **5**, 3924–3931.
- 34 D. Barreca, A. Gasparotto, C. Maragno, E. Tondello, E. Bontempi, L. E. Depero and C. Sada, *Chem. Vap. Deposition*, 2005, **11**, 426–432.
- 35 P. G. Harrison, N. C. Lloyd, W. Daniell, I. K. Ball, C. Bailey and W. Azelee, *Chem. Mater.*, 2000, **12**, 3113–3122.
- 36 Q. H. Xie, Y. Wang, B. Pan, H. M. Wang, W. Y. Su and X. X. Wang, *Catal. Commun.*, 2012, **27**, 21–25.
- 37 D. W. Li, S. X. Ouyang, H. Xu, D. Lu, M. Zhao, X. L. Zhang and J. H. Ye, *Chem. Commun.*, 2016, **52**, 5989–5992.
- 38 J. Zhang, X. Jin, P. I. Morales-Guzman, X. Yu, H. Liu, H. Zhang, L. Razzari and J. P. Claverie, *ACS Nano*, 2016, **10**, 4496–4503.
- 39 J. G. Yu, K. Wang, W. Xiao and B. Cheng, *Phys. Chem. Chem. Phys.*, 2014, **16**, 11492–11501.
- 40 V. Spagnol, E. Sutter, C. Debiemme-Chouvy, H. Cachet and B. Baroux, *Electrochim. Acta*, 2009, **54**, 1228–1232.
- 41 A. Ishikawa, T. Takata, J. N. Kondo, M. Hara, H. Kobayashi and K. Domen, *J. Am. Chem. Soc.*, 2002, **124**, 13547–13553.
- 42 Y. Wang, H. B. Fang, Y. Z. Zheng, R. Q. Ye, X. Tao and J. F. Chen, *Nanoscale*, 2015, **7**, 19118–19128.
- 43 D. T. You, B. Pan, F. Jiang, Y. G. Zhou and W. Y. Su, *Appl. Surf. Sci.*, 2016, **363**, 154–160.
- 44 M. Zeng, X. Zeng, X. G. Peng, Z. Zhu, J. J. Liao, K. Liu, G. Z. Wang and S. W. Lin, *Appl. Surf. Sci.*, 2016, **388**, 352–358.
- 45 S. A. Ansari, M. M. Khan, S. Kalathil, A. Nisar, J. Lee and M. H. Cho, *Nanoscale*, 2013, **5**, 9238–9246.

